Dosimetry of Copper-64-Labeled Monoclonal Antibody 1A3 as Determined by PET Imaging of the Torso

P. Duffy Cutler, Sally W. Schwarz, Carolyn J. Anderson, Judith M. Connett, Michael J. Welch, Gordon W. Philpott and Barry A. Siegel

Divisions of Radiation Sciences and Nuclear Medicine, Mallinckrodt Institute of Radiology, Washington University School of Medicine, St. Louis, Missouri; and Department of Surgery, The Jewish Hospital of St. Louis, St. Louis, Missouri

We present biodistribution and dosimetry results for ^{64}Cu-benzyl-TETA-MAb 1A3 from 15 human subjects injected with this tracer as determined by serial PET imaging of the torso. **Methods:** PET imaging was used to quantify in vivo tracer biodistribution at two time points after injection. Absorbed dosimetry calculated using MIRD-11 and the updated MIRDOSE3 was compared with estimates obtained using rat biodistribution data. **Results:** By measuring activity concentrations in the torso, and extrapolating for the whole body using standard organ and tissue volumes, we were able to account for 93% of the injected radiopharmaceutical over a range of imaging times from 0 to 36 hr postinjection. Based on PET imaging and the MIRD-11 schema, the liver and spleen are the critical organs with average absorbed doses of 0.12 and 0.10 mGy/MBq (0.44 and 0.39 rad/mCi). The revised MIRDOSE3 scheme yields similar values for these and other organs but also results in a dose of 0.14 mGy/MBq (0.53 rad/mCi) to the heart wall. In the rat, the large intestine is the critical organ at 0.14 mGy/MBq (0.52 rad/mCi), while liver and kidneys each receive 0.11 mGy/MBq (0.41 rad/mCi). Some disparities in absorbed doses determined by these methods are evident but are a result of dissimilar biodistributions in rats and humans. For most organs, rat extrapolated values are higher than the human measurements with PET. **Conclusion:** This study shows that torso PET imaging can quantitatively measure the whole-body biodistribution of a radiopharmaceutical as long as it has relatively slow pharmacokinetics.

Key Words: copper-64-antibody; positron emission tomography; torso

J Nucl Med 1995; 36:2363–2371

Use of positron radionuclides has been suggested as a more accurate approach to the determination of radiopharmaceutical dosimetry. For example, ^{94m}Tc has been used as a PET analog of ^{99m}Tc to better determine quantitative dosimetry of routine technetium radiopharmaceuticals (*1*). Also, ^{124}I has been used in a preliminary investigation (n = 1) to evaluate dosimetry with a monoclonal antibody (MAb) specific for neuroblastoma (*2*). In this study, we present multipatient data to evaluate the dosimetry of ^{64}Cu-labeled MAb 1A3, specific for colorectal carcinoma.

Copper-64 offers the advantages of a positron-emitting tracer for imaging and also has potential for use as an internally administered therapeutic radionuclide. Its x-ray, Auger and energetic beta emissions provide effective short-range cell killing (*3*), while a modest positron yield (18%) provides an adequate flux of annihilation photons to allow imaging of the biodistribution by PET. In this study, we exploit the radionuclide's positron imaging capabilities to evaluate MAb 1A3 for detection of colorectal cancer, with the tacit assumption that this radionuclide/antibody combination may ultimately be useful for radioimmunotherapy (*4,5*).

Serial PET imaging to assess total-body biodistribution is facilitated by the use of a relatively long-lived radionuclide such as ^{64}Cu ($T_{1/2}$ = 12.8 hr). With shorter-lived radionuclides, the time necessary to image the entire torso (2–3 hr) precludes repeat whole-body measurements. Acquisition of statistically adequate emission data requires somewhat longer overall imaging times than with ^{18}FDG because of the low positron yield of ^{64}Cu, but only slightly longer since acquisition of the emission events comprises just half the study. High-quality transmission scans are also necessary to derive accurate quantitative information from the study. These may be acquired virtually simultaneously with the emission images, with activity already injected in the patient (*6,7*). Postinjection transmission imaging is accomplished by a set of rotating ^{68}Ge-^{68}Ga rods and an electronic mask that allows the scanner to collect transmitted ^{68}Ge-^{68}Ga photons preferentially rather than emitted ^{64}Cu photons (*8*). With this technique, transmission image quality and

Received Nov. 10, 1994; revision accepted May 16, 1995.

For correspondence or reprints contact: P. Duffy Cutler, PhD, Division of Radiation Sciences, Mallinckrodt Institute of Radiology, 510 S. Kingshighway Blvd., St. Louis, MO 63110.

accuracy actually benefits from a low emission count rate. Still, this type of study is limited by its long measurement time to use with tracers that have slow pharmacokinetics, thus allowing repeat measurements to be spread over a long period following injection, as in this case, from 0 to 36 hr.

The goal of this investigation was to assess the human total-body dosimetry of a positron-emitting radiopharmaceutical compound in a more accurate manner than is possible by extrapolation of rat dissection/biodistribution measurements. Copper-64-labeled MAb 1A3 shows promising results in the diagnosis and localization of colorectal tumors, but its clearance from the blood is slow with virtually no excretion, offering the possibility of large absorbed doses to blood-rich organs such as the heart and spleen. The potential for radioimmunotherapy with this antibody labeled with either ^{64}Cu or ^{67}Cu clearly depends on this determination, so an accurate assessment of dosimetry in humans is essential.

MATERIALS AND METHODS

Human PET Studies

Thirty-six subjects with confirmed colorectal cancer were injected with 5, 10 or 20 mg of MAb 1A3 labeled with ~370 MBq (10 mCi) ^{64}Cu (*9*). An investigational new drug application was filed with the U.S. Food and Drug Administration, and the research protocol was approved by both the Institutional Review Board and the Radioactive Drug Research Committee at Washington University School of Medicine. Each patient gave informed consent before participation in the study. In 15 patients, two imaging studies were performed to facilitate dosimetry. Eleven of the 15 patients were imaged at 4 and 22 hr, two were imaged at 22 and 27 hr, one at 12 and 18 hr and one at 18 and 36 hr postinjection. This mixture of imaging times was chosen to be convenient for patient imaging, while still providing an adequate spread of data points from 0 to 36 hr for dosimetry purposes.

Imaging of the torso, from the pelvis to the shoulders, consisted of four 20-min static emission scans and four 10-min postinjection transmission scans on a Siemens/CTI ECAT EXACT (Knoxville, TN) PET system. Transmission scans were acquired alternately with emission scans to ensure correct alignment. The transmission source consisted of three 92.5 MBq (2.5 mCi) ^{68}Ge-^{68}Ga rotating rods with a positional windowing scheme to minimize contamination by emission photons. Emission subtraction and/or transmission-image segmentation were found to be unnecessary to achieve accurate (±5%) quantitative transmission values with this tracer, so the transmission scans were used directly with modest (10 mm FWHM) axial and transaxial smoothing.

The time necessary to complete the torso imaging procedure is in the range of 3–4 hr, although adequate qualitative images could be obtained in less time by sacrificing statistical precision. Such a long procedure tests the tolerance of even the most compliant patients. Though more imaging sessions in the 36 hr after injection might be desirable from a dosimetry standpoint, we felt that more than two sessions would be unreasonable for most of the sick and aged patients in the study. Thus, it was essential that we be able to combine the data from all patients to form aggregate time-activity curves. As this is not the generally accepted method of measuring the biokinetics of an antibody, we also sought to show that such an aggregation of individuals would reasonably represent the average pharmacokinetics of the antibody in humans. Initially, some normalization of imaging data among patients was anticipated since considerable interpatient variability is known to exist for antibodies like 1A3. Additionally, patients were given different amounts of antibody in an effort to determine the optimum dose for imaging, although no effect on the level of binding could be observed from the PET images. Inspection of the data from the biological samples of blood and urine, and the PET region of interest (ROI) results showed only a modest level of variability, thus the assumption of similar biodistributions among individual subjects is felt to be reasonable.

Scanner Calibration

The sensitive region of the tomograph was calibrated daily using a solid ^{68}Ge-^{68}Ga cylinder, 20 cm in diameter and containing approximately 0.16 μCi/ml total activity. This cylinder activity was cross-calibrated with a water-filled cylinder containing a similar concentration of [^{18}F]fluoride solution. The activity was assayed by the same dose calibrator used to assay patient doses, which was calibrated against a ^{137}Cs sealed reference source. Geometric attenuation correction (*10*), standard delayed-window randoms subtraction (*11*) and the manufacturer's calculated deadtime correction (*12*) were used. Scatter correction was not used because the calibration cylinder and patient have similar scatter distributions. Quantitative accuracy of the calibrated scanner was assessed by scanning a lucite chest phantom containing spheres and a simulated heart chamber with known activity concentrations of ^{18}F and ^{64}Cu. ROI measurements were found to agree consistently (±5%) for ROI diameters larger than 25 mm (3 × FWHM) (Cutler PD, *unpublished data*, 1994).

The above corrections were applied in reconstructing the images (Hann filter, cutoff = 0.8 Nq) along with the isotope branching ratio (0.18) and integrated decay correction, such that image pixels would represent total activity concentration at the time of the start of the scan.

Image Quantification

In viewing the PET image results, activity injected into each patient was seen to accumulate in six primary organs or compartments. The compartments used to describe the biodistribution of the radiopharmaceutical were: blood, liver, kidneys, spleen, bone and other soft tissue. Only organs and tissues containing a visible accumulation of activity were selected for image quantification.

ROIs were drawn to measure total activity concentration in each organ or tissue. Values in five to six adjacent slices were averaged to obtain a reproducible value of activity concentration. The locations and approximate sizes of the ROIs are illustrated in Figure 1. For the liver, spleen, and kidneys, a large elliptical ROI encompassing as much of the organ as possible was used to obtain an average pixel value. To estimate bone activity, a narrow, irregular ROI was drawn to approximate the visible cross-section of the ilium, and the average pixel value was used. For blood activity, the maximum pixel in a large ROI drawn over the left ventricle was used, thereby avoiding partial volume effects, and averaged across five to six adjacent slices to yield a more reproducible result. Soft-tissue activity was taken as the average value in a large elliptical ROI in the region of the buttocks.

Assignment of Activity

All activity must be accounted for to obtain accurate organ dosimetry. To achieve this condition, the following were assumed:

1. All accumulations of tracer visible in the torso were measured directly and any activity outside the torso contained in

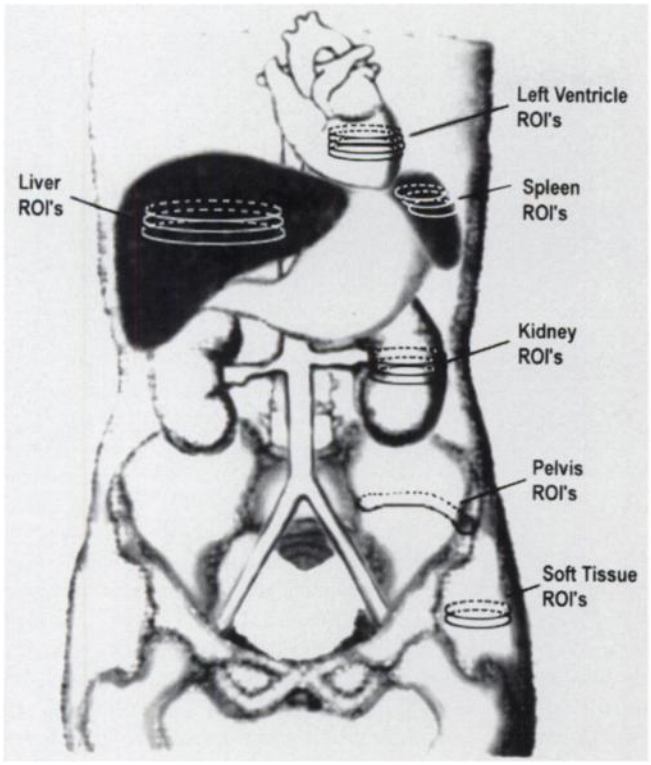

FIGURE 1. Illustration of the ROIs used to extract activity concentrations in blood, liver, kidneys, spleen, bone and soft tissue. Similar activity concentrations outside the torso were assumed for blood, bone and soft tissue. Only organs and tissues containing visible accumulations of tracer were selected for quantification.

blood, bone or soft tissue was assumed to be the same concentration as that within the torso.

2. No accumulation was assumed for the head, neck and legs other than blood pool, bone and soft tissue.
3. Negligible excretion occurs through the urinary bladder or the gastrointestinal tract.

Activity measured in each organ by an image ROI represents both blood and tissue activity. Although these are somewhat separate compartments, we chose to consider them as one. In other words, bloodborne activity within an organ was assigned to the organ as if it were uniformly distributed within it. This is a conservative assumption that will overestimate the organ dose slightly. We estimated that 50%–70% of the energy of emissions from blood-borne ^{64}Cu would be absorbed in an organ such as the liver (*13*), the remainder being absorbed in the blood. Blood activity was also assigned to the heart, lungs and bone marrow, organs for which activity was not measured directly with an ROI. The heart and lungs were assigned a blood fraction based on their respective blood volumes as described below (see Dose Calculations). Assignment of blood activity to the bone marrow was based on the total mass of bone marrow as described below.

Activity measured in bone is assigned half to cancellous (spongy) bone and half to cortical bone. This partitioning is appropriate for the relatively short-lived ^{64}Cu (*14*)*. None of the bone activity is assigned to bone marrow. Instead, red marrow activity is derived from the total blood activity (*15*) as follows:

$$\tau_{marrow} = \tau_{blood} \cdot \left(\frac{m_{marrow}}{m_{blood}}\right) \cdot 30\%. \qquad \text{Eq. 1}$$

The scale factor of 0.3 represents the approximate specific activity of labeled antibodies bound to the surface of the marrow cells, and the masses of marrow and blood are 1120 and 5400 g, respectively. The symbol τ indicates the residence time (see below).

In the MIRD scheme, activity not assigned to a specific organ must be assigned to the remainder-of-body category. In our model, this consists of activity accumulations in soft tissue, unassigned blood and any missing activity. S values for the remainder of body category are calculated based on the total body S values, less the organ-weighted S values for those organs with a specifically assigned activity. The remainder of body (RB) S value for a target organ k is given by:

$$S_{(r_k \leftarrow RB)} = S_{(r_k \leftarrow TB)} \frac{m_{TB}}{m_{RB}} - \sum_h S_{(r_k \leftarrow r_h)} \left(\frac{m_h}{m_{RB}}\right). \qquad \text{Eq. 2}$$

The unassigned blood fraction is determined by subtracting from the total blood volume the blood volume assigned to specific organs. Blood volumes used for this calculation are as follows (*13*): total = 5100 ml, heart = 550 ml, lungs = 300 ml, liver = 250 ml, bone = 190 ml, spleen = 77 ml, kidneys = 72 ml. These organs contain 28% of the blood. Thus, 72% of the total blood activity is assigned to remainder of body.

Blood samples were taken from all 36 patients at roughly 2 and 24 hr postinjection. For our purposes, we considered patient blood samples separately from the PET blood estimates since the percent injected dose (%ID) values from these small samples were determined based on a blood volume normalized to yield 100% ID in the blood at injection. The PET blood measurements were not adjusted in this manner. Only the patient's weight was used in determining the total blood volume. We present both to confirm the shape of the blood clearance curve.

Urine samples were collected as a single accumulated collection over 24 hr following injection and found to contain only 2.2% ± 1.7% ID. In view of this low value, negligible urinary excretion is assumed. "Missing" activity is calculated and included in remainder of body as a conservative assignment of any excreted or unaccounted activity.

Time-activity Curves

The percent injected dose values were calculated by extrapolating the measured activity concentration in each organ to the whole organ using standard organ and tissue volumes (*16,17*). These standard volumes were normalized to each patient's weight. Time-activity curves were then constructed from these values for liver, spleen, kidneys, bone, blood pool and remainder of body. The blood content of each organ was included with the organ where possible rather than assigning it uniformly to the remainder of body. This produces a more accurate estimate of the dose delivered locally to the organ by nonpenetrating radiation, although slightly overestimated, since some of the emissions are absorbed in the blood itself (*18*). Data from all patients were plotted together (excluding physical decay) and fitted by a least-squares regression to achieve a minimum correlation coefficient and to ensure intersection with appropriate values of %ID at t = 0. Initial values used for time-activity curves were actually at t = 0^+ (just after injec-

*The current understanding of antibody binding in bone is that eventually 80% is nonspecifically bound to cortical bone and 20% to cancellous bone. This partitioning is used only if the half-life of the radionuclide is greater than 15 days. For shorter-lived radionuclides, a 50/50 partitioning is used.

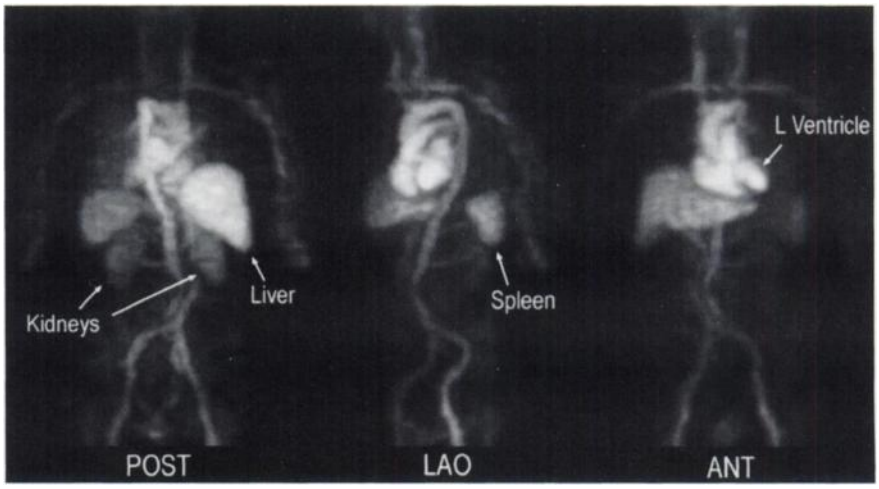

FIGURE 2. Reprojected image volume shows anterior, posterior and left anterior oblique views of the torso 22 hr postinjection. The image volume consists of four separate 20-min acquisitions, each with 47 transaxial slices covering 16.2 cm of the patient's torso. The reconstructed, attenuation-corrected images are stacked together with a 1.7-cm overlap to account for reduced sensitivity in the end planes of the PET scanner.

tion). It was assumed 100% of the activity was in the blood at this time, and instantaneous mixing occurred upon injection. Thus, initial values were based on the known blood volume of each organ. For example, the liver blood volume is 250 ml in a 70-kg man, thereby containing 5% ID at $t = 0^+$. The remainder of body contains 72% of the blood volume as discussed above, thereby containing 72% ID at $t = 0^+$.

Residence Times

Residence times for each organ or tissue were obtained by analytical integration of the time-activity curves. Each least-squares fit is integrated from 0 to ∞ after first multiplying by the physical decay of ^{64}Cu. The fit excludes physical decay of ^{64}Cu so that biological trends will be more clearly evident. In determining the residence time, however, physical decay must be included. For the blood pool, the equation is:

$$\%ID(t) = 67 \cdot (0.5 \cdot e^{-0.35t} + e^{-0.0048t}). \quad \text{Eq. 3}$$

With physical decay, this becomes:

$$\frac{A(t)}{A_0} = 0.67 \cdot e^{-\lambda_{Cu}t} \cdot (0.5 \cdot e^{-0.35t} + e^{-0.0048t}). \quad \text{Eq. 4}$$

After integration, the residence time is given by:

$$\tau = \frac{1}{A_0}\int_0^\infty A(t)dt \quad \text{Eq. 5}$$

$$\tau = 0.68 \cdot \left(\frac{0.5}{\lambda_{Cu} + 0.35} + \frac{1}{\lambda_{Cu} + 0.0048}\right) = 12.11 \text{ hr}.$$

Dose Calculations

Once the residence times are determined for each organ or tissue measured, their values may then be divided up to assign activity to organs not measured directly by ROIs. For example, this technique was used to assign activity to the lungs, bone marrow and the contents of the heart chambers by subtracting cumulated activity from the blood. A fraction of the residence time from the total blood pool (12.11 hr) was assigned to each of these organs based on their respective blood volumes as previously described. The remaining residence time for blood was then assigned uniformly to the remainder of body.

Dose calculations were performed using both the original MIRD 11 S values (*17*) and the updated MIRDOSE3 S values (*18*). The updated version contains additional source and target organs, including heart contents and bone surfaces. Total absorbed doses for each target organ are calculated by tallying the absorbed dose per unit of injected activity (residence time/S value product) for all organs and tissues containing activity. A summary of the organs and their residence times is shown in Table 2 for the two MIRD schemes. Comparison of the integrated residence times shown in Figure 3 and the residence times in Table 2 show where measured blood and bone activity have been reassigned.

Absorbed dose estimates were also calculated for ^{67}Cu-TETA-MAb 1A3, an impurity present in 0.85% concentration at injection. This negligible impurity is only of concern because of the much longer half-life of ^{67}Cu ($T_{1/2}$ = 61.7 hr).

Rodent Studies

Prior to human use, the biodistribution of this radiopharmaceutical was studied in rats to determine approximate dosimetry. A complete description of these measurements can be found in the report of Anderson et al. (*19*). Briefly, six groups of four rats were injected with 186 μg/kg ^{64}Cu-benzyl-TETA-MAb 1A3 and euthanized at 1, 3, 6, 12, 24 or 36 hr, respectively. Samples of 11 different organs or tissues were removed, weighed and counted. Plots of the percent injected dose per gram and percent injected dose per organ as a function of time after injection were generated for each organ, from which residence times (μCi-h/organ) were determined by measuring the area under a smooth curve, assuming only physical decay after 36 hr. These values were assumed to be predictive of the pharmacokinetics in humans and used with the MIRD-11 S values to estimate the absorbed dose to various organs.

RESULTS

Activity Distribution

Figure 2 shows an example of the biodistribution in a human subject obtained 22 hr after injection of 370 MBq (10 mCi) ^{64}Cu-benzyl-TETA-1A3. In the hamster tumor model, we have found maximum tumor uptake of the antibody occurs at approximately 24 hr (*19*); however, our human PET results show that more than 60% of the injected activity is still in the blood at this point. The heart and large vessels are clearly visible. Table 1 shows the fractional distribution of the activity as determined by ROI measurements.

TABLE 1
Approximate Biodistribution of Copper-64-Benzyl-TETA-MAb 22 Hours Postinjection

Compartment	ROI	%ID
Liver + blood	Liver (portion) - avg.	13
Kidneys + blood	Kidneys (whole) - avg.	1
Lungs + blood	(from blood)	4
Spleen + blood	Spleen (portion) - avg.	1
Bone + blood	Pelvis (ilium) - avg.	9
Heart contents	(from blood)	6
Marrow	(from blood)	4
Remainder of body		
Unassigned blood	Left ventricle (whole) - max.	43
Soft tissue	Gluteus maximus - avg.	12
Missing	—	7

No accumulations are visible in the intestinal tract or the urinary bladder, indicating that neither the labeled antibody nor its metabolites are readily cleared from the blood by either hepatobilliary or renal excretion. Activity in the kidneys and spleen is primarily blood-pool activity since these organs are equally visible throughout the imaging period.

As can be seen from Table 1, nearly half the activity is found in the blood pool even as late as 22 hr after injection. Roughly 25% is found in the liver and bone, and the remaining 20% is distributed uniformly throughout the body, where the antibody is bound nonspecifically.

Time-activity Curves

Time-activity curves derived from torso PET images of 15 patients are shown in Figure 3. Figure 4 shows the blood time-activity curve for all 36 patients determined from samples taken at 2 and 24 hr.

The scatter plots were fitted with mono- or bi-exponential functions to yield the best possible correlation coefficient (R) with the constraint that the curve should pass through an appropriate value of %ID at t = 0. In the case of Figure 4, the time constants were constrained to be the same as the values in Figure 3A. The resulting analytic functions are shown in each plot legend. Some parameters for the blood curve were fitted and then fixed to allow other parameters to vary on subsequent fits. This was found to be the best means for guiding the nonlinear regression toward a minimum correlation coefficient.

As a measure of sensitivity to perturbation, freely varying fits of similar functions were performed to a pair of data points representing the worst-case outliers for each organ. This produced, at most, an 8% deviation (blood pool) in the residence time, the integral of the curve, compared with the aggregate fit.

Residence Times

Residence times obtained from the curves shown are as follows: total blood pool = 12.11 hr, liver = 2.18 hr, bone = 1.48 hr, remainder of body = 11.04 hr, spleen = 0.20 hr and kidneys = 0.25 hr. These values were assigned to appropriate MIRD source organs as shown in Table 2. Bone residence time was split evenly between cortical and trabecular bone as discussed above, and the red marrow residence time was determined from the blood residence time according to Equation 2.

Absorbed Dose

Results of the MIRD 11 and MIRDOSE3 dose calculations are shown in Table 3 for both the human PET measurements and the rat biodistribution measurements. The rat data include residence times from 11 source organs compared with 9 for the PET measurements. Both sets of data included all organs that showed substantial activity accumulations.

Blood-rich organs (heart wall, liver, spleen, kidneys and lungs) receive the highest doses according to both human and rat-extrapolated data. The lower large intestine also receives a substantial dose according to the rat-extrapolated data, a feature not evident in the human PET measurements.

DISCUSSION

Copper-64-benzyl-TETA-1A3 monoclonal antibody selectively targets colorectal carcinoma with high immunoreactivity (IR=85–95%) (*19*). Results of our Phase I clinical trial indicate promise in the localization of tumors of the abdomen and pelvis by PET (*9,20*). These results suggest a slightly better specificity for colorectal tumors than ^{18}FDG. A description of the antibody and the techniques used for its conjugation and labeling can be found elsewhere (*19*).

Much of the radiopharmaceutical remains in the blood throughout the imaging period (0–36 hr). This is typical of intact antibodies and is cause for concern from a dosimetry standpoint since several organs, such as the heart and spleen, are chronically exposed to ^{64}Cu emissions. Fortunately, fragments of this antibody are cleared much more rapidly from the blood (*21*) and offer promise as a potentially better substrate in this regard. Although the intact antibody remains in the blood for a period of time, the dose to radiosensitive organs like the lungs and bone marrow is still moderate as these organs do not accumulate the radiopharmaceutical. The liver is the only organ that shows any affinity for ^{64}Cu-TETA-1A3. Hepatic cells appear to internalize or otherwise trap the compound, but no excretion into the gallbladder or bowel lumen is apparent. Liver accumulation approaches 15% ID, reducing the effectiveness of this tracer for detecting hepatobilliary lesions. The labeled fragment of this antibody, ^{64}Cu-1A3-F(ab′)$_2$, however, does not behave this way (*21*), indicating that this accumulation is not due to specific binding in the liver.

The time-activity curves shown in Figure 3 illustrate the kinetic biodistribution of the antibody with physical decay of the ^{64}Cu removed. The blood clearance curve determined from blood samples in Figure 4 yields regression parameters very similar to the PET blood clearance curve. The data in Figure 4 were fit with the same function and with the constraint of the identical time constants used in Figure 3A. This was done to preserve the shape of the

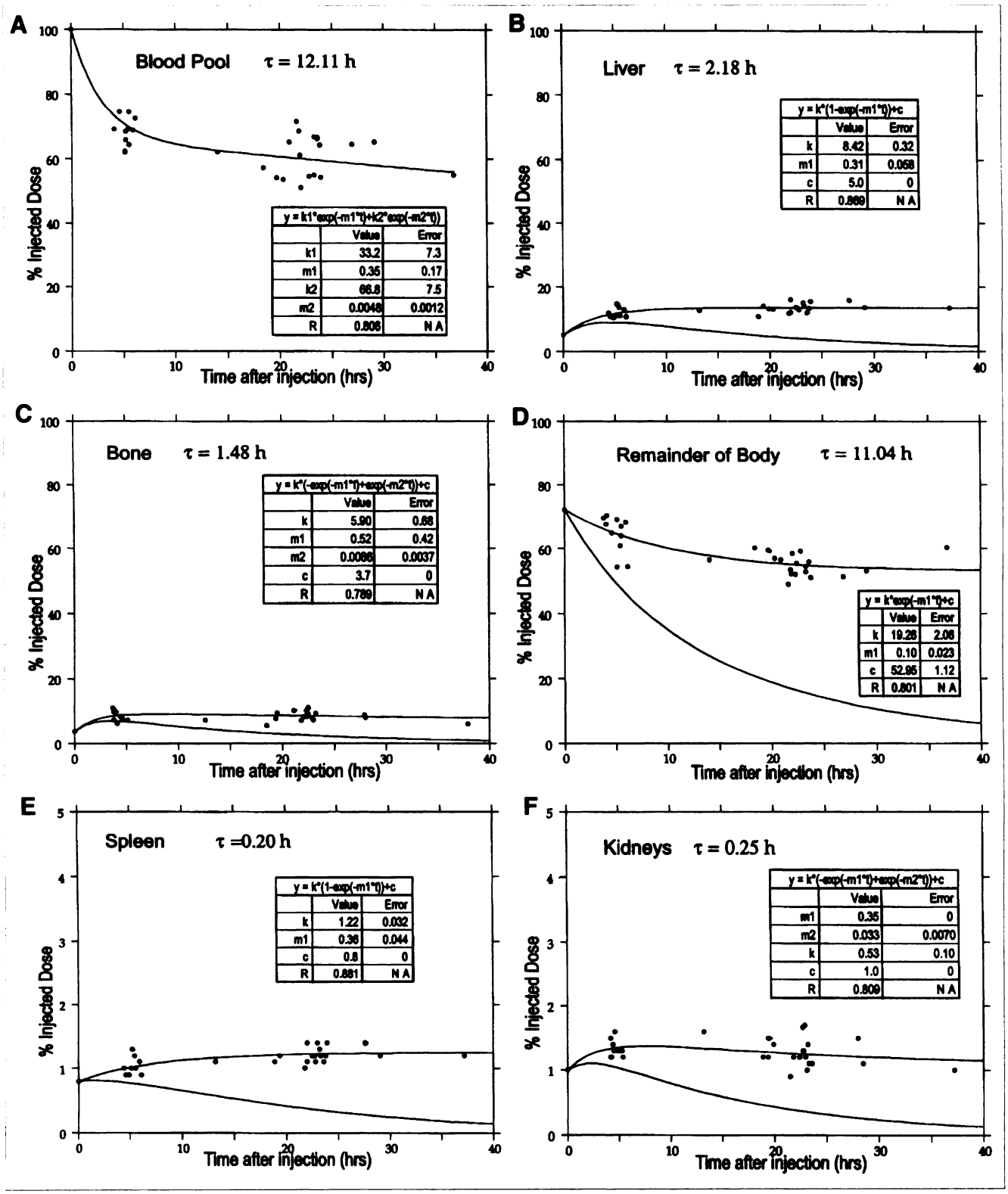

FIGURE 3. Percent injected dose of ^{64}Cu-benzyl-TETA-1A3 in 15 human subjects as determined by PET imaging for: (A) blood, (B) liver, (C) kidneys, (D) spleen, (E) bone and (F) remainder of the body. Also shown are least square fits with mono- or bi-exponential functions. Functional forms are integrated to determine average residence times for each compartment. Values are then assigned to the eight MIRD source organs in Table 2.

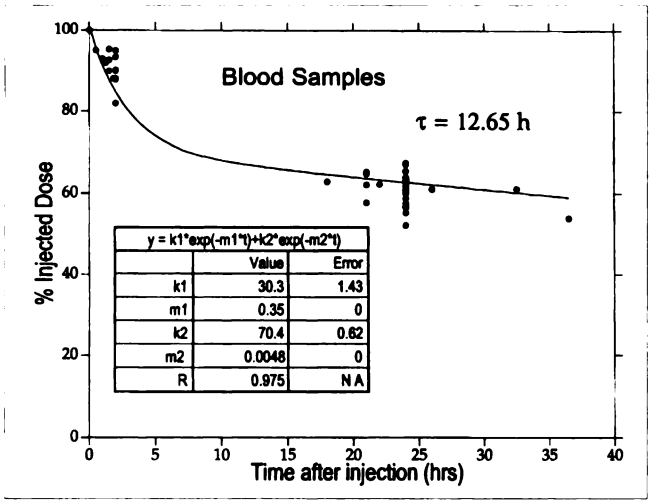

FIGURE 4. Percent injected dose of ^{64}Cu-benzyl-TETA-1A3 in blood determined from blood samples counted in vitro. Total blood volume is estimated as 70 ml/kg body weight and then adjusted to yield 100% ID at injection.

blood curve from a decidedly better distribution of time points in the PET data. The remaining coefficients are within the standard error when this technique is used, and the residence time of the curve is 4% greater. Without constraining the time constants, the fit produces a slightly flatter curve and the residence time is 12.75 hr (5% greater than the PET result).

Scatter of the data points gives a good indication of the uptake variability among the 15 patients. In general, organs show narrow distributions, with the exception of blood pool, which shows a somewhat broader distribution at 20–24 hr. The narrow distribution of the remainder of the body values, which consist of blood-pool, soft tissue and missing activity, means that the absorbed dose estimates will be consistent among patients. High variability of blood activity values but low variability of remainder of body values are evidently a result of variable nonspecific binding in the soft tissues. Though interesting, this is not significant in terms of the resulting absorbed dose values, since both blood and soft tissue are assigned to the remainder of the body under the MIRD scheme. Correlation coefficients for the fits in Figure 3 are all in the range of 0.8, and standard error estimates are reasonable, indicating that the regression fits are stable and not sensitive to large perturbation errors. The blood-pool residence time could be varied by only 8% when a selected pair of outlier data points were fit. This variability was less than 5% for all other organs.

Bladder activity was monitored cumulatively in this investigation. Whereas this radiopharmaceutical has low urinary excretion, allowing it to be neglected for dosimetry purposes, this will not generally be the case. The methods described here for image-based activity quantification can easily be extended to measure bladder activity. In dosimetry studies with other radiopharmaceuticals, we have found the combination of image measurements and physiological samples to be self-consistent and therefore accurate. Simple assumptions such as a 90% void fraction for a voluntary void, or 95% for a catheter extraction can easily be validated with images before and after the void. With these assumptions, urine samples for each void and a few well-chosen imaging times, a detailed time-activity curve can be constructed for the bladder.

TABLE 2
Assignment of Activity in MIRD Source Organs

Organ	MIRD 11 Residence time (hr)	MIRDOSE3 Residence time (hr)
Heart contents	—	1.30
Liver	2.18	2.18
Kidneys	0.25	0.25
Lungs	0.72	0.72
Spleen	0.20	0.20
Bone		
Cortical	0.74	0.74
Cancellous	0.74	0.74
Red marrow	0.76	0.76
Remainder of body	12.09	10.79

CONCLUSION

The technique of torso PET imaging provides a superbly noninvasive means of measuring the biodistribution of a new, positron-labeled radiopharmaceuticals and has clearly helped facilitate the introduction of these compounds. Part of this development has come from the longer axial field of view available with some current generation PET tomographs, enabling large-area surveys of the torso or the whole body in a period of time short enough to avoid tracer redistribution during the measurement. As with single-organ PET studies, the resulting images can be calibrated to yield absolute quantitative results with a minimum of effort. The result is an image volume that provides visualization of all essential organs simultaneously as well as a quantitative assessment of radiopharmaceutical biodistribution.

In the case of ^{64}Cu, which has a positron yield of only 18%, illustrates the sensitivity with which PET can accomplish this task. Whereas the total injected activity may be limited to 370 MBq (10 mCi) for total-body dose considerations in humans, an injection of less than 74 MBq (2 mCi) of a positron-emitting label still yields a count rate sufficient to image the torso in 90–120 min. While this provides relatively poor temporal resolution, it is adequate for many compounds. Time-activity measurements may be obtained on one or several subjects for all organs and tissues that accumulate substantial activity. These data can be easily tailored to suit the MIRD source organs to allow accurate absorbed dose estimates.

With the ongoing development of quantitative three-dimensional PET imaging, the long acquisition time can be substantially reduced once accurate attenuation, scatter and deadtime compensation methods are developed to provide quantitative volumetric images (*22–24*). For these investigations, we have used the two-dimensional acquisition

TABLE 3
Comparison of Human Absorbed Dose Estimates from Copper-64-Benzyl-TETA-MAb Based on Rat Biodistribution Data and Results of Human Torso PET Imaging

Organ or tissue	Rat dissection mGy/MBq (rads/mCi)	Human PET-MIRD 11 mGy/MBq (rads/mCi)	Human PET-MIRDOSE3 mGy/MBq (rads/mCi)
Heart wall	—	—	0.14 (0.53)
Liver	0.11 (0.41)	0.12 (0.44)	0.11 (0.41)
Spleen	0.06 (0.23)	0.10 (0.39)	0.09 (0.35)
Kidneys	0.11 (0.42)	0.08 (0.30)	0.08 (0.29)
Red marrow	0.08 (0.28)	0.06 (0.24)	0.08 (0.30)
Lungs	0.05 (0.19)	0.07 (0.27)	0.07 (0.26)
Bone (Surfaces*)	—	0.03 (0.12)	0.06 (0.21)
Upper large intestine	0.08 (0.31)	0.03 (0.11)	0.02 (0.08)
Lower large intestine	0.14 (0.52)	0.03 (0.10)	0.02 (0.08)
Small intestine	0.03 (0.22)	0.03 (0.11)	0.02 (0.09)
Muscle	0.03 (0.10)	0.02 (0.09)	0.02 (0.08)
Whole body	0.03 (0.11)	0.03 (0.11)	—

*MIRDOSE3 determines absorbed dose to bone surfaces.

mode exclusively. Since the total imaging time can approach or exceed 2 hr, image quality is limited by patient tolerance but is clearly adequate for tumor localization and dosimetry.

Despite the prolonged blood-pool activity, our calculations show only moderate absorbed doses to the heart, lungs and bone marrow. Fortunately, no accumulation except that in the blood is evident in these organs. The disparity between absorbed doses to the intestines in humans and rats is due to the substantially different biodistributions in these two mammals. This difference is not surprising, as substantial differences in the distribution of many radiopharmaceuticals are common among members of the same mammalian order. The rat apparently clears the antibody (or a degradation product) through the gastrointestinal tract, whereas virtually no activity other than in the blood is evident in the lower abdomen in human PET studies.

The MIRDOSE3 scheme agrees well with the MIRD 11 values and also shows a high dose delivered to the heart wall. A significant dose to the heart wall is intuitively reasonable since the tracer chiefly resides in the blood. MIRDOSE3 also calculates a dose to the bone surfaces rather than to total bone. Recent investigations have shown that particularly high energy deposition occurs at the bone-soft tissue interfaces due to the abrupt change in density (*18*). These additional pieces of data illustrate the advantage of the more comprehensive list of source and target organs available with MIRDOSE3.

In this study, we have determined the normal organ dosimetry of ^{64}Cu-MAb-1A3. These data, along with accurate tumor dosimetry, will form the basis for investigations of therapeutic use of monoclonal antibodies labeled with ^{67}Cu or ^{64}Cu.

ACKNOWLEDGMENTS

This work was supported by National Institutes of Health grant CA44728 and a grant from the Whitaker Foundation. The authors are grateful for many helpful discussions with M. Stabin and J. Stubbs of the Radiation Internal Dose Information Center, Oak Ridge, TN and J. O. Eichling, Radiation Safety Officer and professor of radiology at Washington University.

REFERENCES

1. Nickles RJ, Nunn AD, Stone CK, Christian BT. Technetium-94m-teboroxime: synthesis, dosimetry and initial PET imaging studies. *J Nucl Med* 1993;34:1058–1066.
2. Larson SM, Pentlow KS, Volkow ND, et al. PET scanning of iodine-124-3F8 as an approach to tumor dosimetry during treatment planning for radioimmunotherapy in a child with neuroblastoma. *J Nucl Med* 1992;33:2020–2023.
3. Grisvard J, Guile E, Sasaki I, et al. Biochemical studies of human (A549) and simian (CV1) cells labeled with Cu-64, Cu-67 and I-125-IUdR. *Biological Trace Element Research* 1989;20:207–224.
4. Connett JM, Guo LW, Anderson CJ, J WM, Philpott GW. Radioimmunotherapy of human colon carcinoma (GW-39) in hamsters with Cu-67 anti-colon cancer monoclonal antibody (MAb) 1A3 [Abstract]. *Cancer Res* 1994; 35:649.
5. Anderson CJ, Connett JM, Guo LWea. Initial comparison of Cu-67- and Cu-64-labeled anticolorectal carcinoma MAb 1A3 as agents for radioimmunotherapy in tumor-bearing hamsters [Abstract]. *J Nucl Med* 1994;35(suppl): 161P.
6. Thompson CJ, Ranger NT, Evans AA. Simultaneous transmission and emission scans in positron emission tomography. *IEEE Trans Nucl Sci* 1989;36: 1011–1016.
7. Ranger NT, Thompson CJ, Evans AC. The application of a masked orbiting transmission source for attenuation correction in PET. *J Nucl Med* 1989;30: 1056–1068.
8. Jones WF, Digby WM, Luk WK, Casey ME, Byars LG. Optimizing rod window width in positron emission tomography. *IEEE Medical Imaging Conference*. 1992:982–984.
9. Philpott GW, Schwarz SW, Anderson CJ, et al. RadioimmunoPET: Detection of colorectal carcinoma by positron emission tomography with a Cu-64-labeled monoclonal antibody. *J Nucl Med* 1995;36:1818–1824.
10. Huang SC, Hoffman EJ, Phelps ME, Kuhl DE. Quantitation in positron emission tomography: II. Effect of inaccurate attenuation correction. *J Comput Assist Tomogr* 1979;3:804–814.
11. Hoffman EJ, Huang SC, Phelps ME, Kuhl DE. Quantitation in positron

emission tomography: IV. Effect of accidental coincidences. *J Comput Assist Tomogr* 1981;5:391–400.
12. Germano G, Hoffman EJ. Investigation of count rate and deadtime characteristics of a high-resolution PET system. *J Comput Assist Tomogr* 1988;12: 836–846.
13. Cloutier RJ, Edwards CL, Snyder WS. Radiation dose from radioisotopes in the blood. In: Anderson EB, ed. *Medical radionuclides: radiation dose effects*. Oak Ridge, TN: Oak Ridge Associated Universities; 1970:325–345.
14. Stubbs J. Bone dosimetry modeling. Radiation Internal Dose Information Center: Oak Ridge Institute for Science and Education, 1994.
15. Siegel JA, Wessels BW, Watson EE, et al. Bone marrow dosimetry and toxicity for radioimmunotherapy. *Antibody Immunocon Radiopharm* 1990;3: 213–233.
16. Snyder WS, Fisher Jr HL, Ford MR, Warner GG. Estimates of absorbed fractions for monoenergetic photon sources uniformly distributed in various organs of a heterogeneous phantom. MIRD pamphlet no. 5. *J Nucl Med* 1969;10(S3):5–12.
17. Snyder WS, Ford MR, Warner GG, Watson SB. "S," absorbed dose per unit cumulated activity for selected radionuclides and organs. *MIRD pamphlet no. 11*. New York: Society of Nuclear Medicine; 1975.
18. Stabin M. MIRDOSE3: radiation dose estimates for the reference adult for Cu-64. Radiation Internal Dose Information Center: Oak Ridge Institute for Science and Education, Oak Ridge, TN, 1994.
19. Anderson CJ, Connett JM, Schwarz SW, et al. Copper-64 labeled antibodies for PET imaging. *J Nucl Med* 1992;33:1685–1691.
20. Philpott GW, Dehdashti F, Schwarz SW, et al. Positron emission tomography (PET) with Cu-64-labeled monoclonal antibody (MAb 1A3) in colorectal cancer [Abstract]. *J Nucl Med* 1994;35:12P.
21. Anderson CJ, Schwarz SM, Connett J, et al. Optimization of copper-64-labeled monoclonal antibody (MAb) fragments 1A3-F(ab')$_2$ for PET imaging of colorectal cancer. *J Nucl Med* 1995;36:850–858.
22. Bailey DL. Three-dimensional acquisition and reconstruction in positron emission tomography. *Ann Nucl Med* 1992;6:123–130.
23. Cherry SR, Dahlbom M, Hoffman EJ. High sensitivity total-body PET scanning using three-dimensional data acquisition and reconstruction. *IEEE Trans Med Imag* 1992;39:1088–1092.
24. Defrise M, Townsend DW, Bailey D, Geissbuhler A, Michel C, Jones T. A normalization technique for three-dimensional PET data. *Phys Med Biol* 1991;36:939–952.